

## **Magnetic Vectoring of Magnetically Responsive Nanoparticles (MNP) within the Murine Peritoneum**

**Jim Klostergaard<sup>1</sup>, James Bankson<sup>1</sup>, William Yuill<sup>2</sup> and Charles E. Seeney<sup>2</sup>**

<sup>1</sup>The University of Texas, MD Anderson Cancer Center, Houston, TX and <sup>2</sup>NanoBioMagnetics, Inc.,  
Edmond, OK USA

**Abstract:** Magnetically responsive nanoparticles (MNP) might be candidates for pro-drug formulations for intraperitoneal (i.p.) treatment of ovarian cancer. We have conducted feasibility experiments in a human ovarian carcinoma i.p. xenograft model to determine whether MNPs can be effectively vectored within this environment. Our initial results based on magnetic resonance imaging indicate that i.p.-injected, ~15 nm magnetite-based MNPs can in fact migrate toward Nd/B/Fe magnets externally juxtaposed to the peritoneal cavity; when the magnets are juxtaposed over an i.p. xenograft growing in the anterior abdominal wall, MNP localization to the tumor/peri-tumoral environment occurs. Further development of this MNP pro-drug strategy is underway.

**Key words:** Magnetically Responsive Nanoparticles, pro-drug, intraperitoneal, human ovarian carcinoma, xenografts

Dr. Jim Klostergaard  
Department of Molecular & Cellular Oncology  
The University of Texas  
MD Anderson Cancer Center  
Houston, TX 77030  
FAX: 713-794-0209  
Phone: 713-792-8962  
[jkloster@mdanderson.org](mailto:jkloster@mdanderson.org)

**Introduction:** Ovarian cancer is the most lethal gynecological malignancy. In the United States, it is the fourth leading cause of cancer deaths in women, with >25,000 new cases and >16,000 deaths annually (1); in the United Kingdom (2) and Europe (3-5), the impact is on a similar scale.

The real problem with ovarian cancer is its silent progression. Unlike the situation with other solid tumors in which screening and early detection have made a great impact on survival, there is no accepted diagnostic that can be effectively applied to general population screens. For example, although CA125 is a mainstay of monitoring and assessing treatment response and patient relapse in the setting of such known disease, it has insufficient sensitivity and specificity to serve as a screen (1, 6-8).

Until this situation changes, regrettably ~75% of newly diagnosed cases will be at stage III/IV, with peritoneal disease (carcinomatosis) and distant metastases. Carcinomatosis presents a unique tumor biology, and although most women respond to initial chemotherapy following post-debulking surgery, almost invariably relapsing disease occurs, that is, confoundingly, increasingly chemo-resistant. Hence, the dismal 5-year survival rates for this stage of the disease have not changed significantly over decades from the 15-30% range (1-5).

However, recent clinical trials provide potentially practice-altering evidence for the survival benefit from intraperitoneal (i.p.) vs. intravenous (i.v.) chemotherapy (CTX; 9-12). The most compelling of these trials demonstrated a survival improvement of ~16 months, with i.p. compared to i.v. arms, an enormous impact considering the usual timeline (12). Despite its greater toxicity, i.p. CTX is highly likely to become the accepted approach, rather than one of purely experimental interest reserved for technology-rich, large cancer centers.

We are thus lead to hypothesize that the free taxane and platinum drugs currently used in such i.p. CTX therapy regimens for ovarian cancer would provide even greater patient benefit if they could be tumor-targeted; and for this purpose, we believe that magnetically-vectored, drug-loaded nanoparticles (NPs) merit development and evaluation in relevant pre-clinical models. The initial steps on this path are the subjects of the current studies.

**Experimental:** For these purposes, we have focused on using silica-coated, single-domain, superparamagnetic magnetite ( $\text{Fe}_3\text{O}_4$ ) nanoparticles NPs, typically 15-20 nm in diameter, as previously described (13). Several parameters must be balanced in arriving at this choice of MNP as the initial point for evaluation. First, their magnetic susceptibility, a direct function of the mass of magnetite in the MNP, must be adequate to respond to magnetic field gradients achievable with readily available (commercial) magnets: thus, favoring larger particles. Although vectoring within the peritoneum is not likely to encounter the magnitude of flow environments that exist in normal or tumor vasculature (14), sufficient force must still be achieved to traverse the distances and obstacles within the cavity. In contrast, other considerations favor the use of smaller particles, including the possibilities of unique modes of passage through cells claimed to occur at the nanoscale, and the ability to move around visceral organ barriers within the peritoneum. Finally, the silica coating enhances MNP biological stability and inertness, reduces MNP-MNP interactions, and allows access to a rich Si-based chemistry for MNP conjugation to drug payloads and affinity-based targeting moieties, as well. It should be noted, however, that the issues of particle stability and possible particle toxicity are interlinked, and it may be that exploiting normal clearance mechanisms will require some additional modification to these MNP.

The first experiments with these MNPs we conducted were in normal (non-tumor-bearing) female nude mice, the hosts for subsequent experiments with implanted human ovarian carcinoma xenografts. These experiments were intended to determine whether these MNPs demonstrated sufficient magnetic susceptibility to move under the influence of the fields from readily available permanent magnets. Because these particles also function as ultra-small paramagnetic iron oxides (USPIOs), a class of contrast agents that are known to cause easily recognizable artifacts in magnetic resonance imaging (MRI) measurements, MRI was used to non-invasively visualize the distribution and movement of particles over time. All MR measurements were made using a 4.7T Biospec small animal MRI system (Bruker Biospin MRI, Billerica, MA) with standard gradient (60mm I.D.) and volume RF coil (35mm I.D.) configurations. Animal anatomy and particle distribution was visualized using multi-slice T1- (TE/TR 8.5/620ms), T2- (TE/TR 60/300ms), and multi-echo T2\*-weighted (TE/TR 3.5,12.2,20.9/500ms, 45° flip angle) sequences along with a 3-dimensional T1-weighted (TE/TR 2.5/50ms, 30° flip angle) acquisition. For multi-slice acquisitions, a field-of-view (FOV) of 50 x 37.5mm was acquired over a matrix of 256 x 192

points with a slice thickness of 1mm and an 0.25mm gap between slices. The FOV of the 3-dimensional scans was 50 x 37.5 x 24mm over a matrix of 256 x 192 x 24 points.

Following *in vitro* magnetic resonance imaging (MRI) phantom experiments to determine what concentrations of particles were likely to be effective in causing image artifacts *in vivo*, 150  $\mu$ L of 1000  $\mu$ g/ml concentrations of these MNPs were injected i.p., followed immediately by placement of a 22 mm diameter cylindrical Nd/B/Fe magnet (Arbor Scientific), rated at 5600 Gauss at its face surface, to the right of the mouse abdomen for 2 hr; during this time, the mouse was resting on its anterior, under monitored isoflurane inhalation anesthesia. Control mice did not have a magnet in place, but otherwise were treated the same and for the same duration. Coronal and sagittal, T1-, T2-, and T2\*-weighted MR images were obtained pre-injection and immediately following the magnetic localization.

Representative T1-weighted, 3-dimensional coronal images are shown in **Figure 1**. The image on the left is taken pre-injection, showing normal peritoneal anatomical features in this slice. The image in the middle is taken after a mouse was injected with MNPs and left under anesthesia with no magnet in place for 2 hr; it shows wide dispersion of the MNPs left in the peritoneum. The image on the right is from a mouse similarly injected, but with the magnet placed to the right (left on image) of its abdomen. MR evidence for accumulation of MNPs near the juxtaposed magnet is clear. Thus, we were confident that the magnetic susceptibility of these MNPs and the field strength of this magnet were sufficient to cause MNP movement within the dimensions relevant to the peritoneum of a normal mouse.

With this capability ascertained, we next began studies in a tumor-bearing mouse. The tumor model we focused on initially is the HEY human ovarian carcinoma. In contrast to the poly-focal presentation of carcinomatosis, characteristic of initial presentation of Stage III disease, the HEY i.p. xenograft grows focally, with frank disease within the peritoneum, and also with a major, primarily solitary lesion in the injection needle-track in the anterior abdominal wall, that progresses to invade the peritoneum. This is more akin to the focal disease that can occur with relapsing disease, and we elected to start with this scenario.

In the first experiment in this model, we i.p.-injected an identical load of MNPs to that used in the preceding normal mouse study; these MNPs were also labeled with FITC to allow post-mortem particle localization by fluorescence microscopy to be conducted on tissue sections. In this setting, the same cylindrical magnet was suspended above the mouse abdomen with the anesthetized mouse lying on its back for 2 hr immediately post-MNP injection; the cylinder axis was aligned with and the magnet face placed proximally to the i.p. tumor needle track from tumor cell inoculation two-three weeks earlier, as this growth was evident subcutaneously on the abdomen. The control, tumor-bearing mouse did not use this magnet for the same duration; due to the position of the tumor in the abdomen, sagittal rather than coronal T1- and T2-weighted MR images were obtained, as this offered a better view.

The resulting T1- and T2\*-weighted images are shown in **Figure 2**. The two images on the top are taken 2 hr post-injection, without a magnet in place over the anesthetized mouse: the T1-weighted image on the right showing the prominent outline of the tumor in the anterior abdominal wall, and the T2\*-weighted image on the left showing little discernable evidence for MNP accumulation in any tissue in this slice. The three images on the bottom are taken 2 hr post-injection, with the magnet in place over the tumor of the anesthetized mouse for the full duration. The T2\*-weighted image on the left shows marked signal ablation due to MNP accumulation in the tumor/peri-tumoral area and neighboring abdominal wall. The yellow scalar is inserted for orientation of the distance between bladder and tumor centers on this image and the image in the middle. The two T1-weighted images in the middle and right display clear susceptibility artifacts characteristic of signal distortion due to USPIOs; the middle image again shows the yellow scalar for orientation, as well as a red marker for the tumor center, while the image on the right is native. Thus, based on these MR imaging results, it seems clear that these MNPs can be vectored to the tumor/peri-tumoral area in this model. More exact tissue and cellular localization is currently being analyzed by histology/fluorescence microscopy.

We recognized that, although there was convincing MRI evidence for significant movement of the MNPs to the tumor/peri-tumoral area, there was also substantial accumulation apparent near normal tissues such as the abdominal wall, likely due to the wide bore of the magnetic field of this 22 mm magnet. Since this would likely be a source of future toxicity if these MNPs were drug-loaded, we attempted to determine whether use of a similarly-powered, but more focused magnetic field, might improve MNP localization. For this purpose, we used a pyramid-shaped magnet (K and J Magnetics) that has a flat peak surface of  $\sim 3$  x

3 mm. In every other respect, the next experiment was conducted identically to the preceding one with the cylindrical magnet, and the resulting images (all post-magnet vectoring) are shown in **Figure 3**. The images on the left vs. right are from neighboring slices, and the upper images are T2-weighted, whereas the lower images are T2\*-weighted and more prone to distortion in the presence of these particles. By comparison of these T2\*-weighted images to that on the bottom left of **Figure 2**, we concluded that the use of the more focused magnet caused less undesired MNP localization to the normal tissues of the abdominal wall, while still achieving accumulation to the HEY tumor or peri-tumoral area. As stated before, histological analyses will be required for more definitive conclusions as to the precise tissue location of the MNPs.

Since the HEY tumor model demonstrated early, focal growth, and rapidly acquired significant size that should require angiogenesis, we reasoned that i.v. administration of MNPs, followed by magnetically-enhanced extravasation, would merit evaluation as an effective means of tumor delivery to a peritoneal tumor. We had not previously established the pharmacokinetic behavior of these MNPs, particularly in the plasma; therefore, it was uncertain whether, without purposely endowing the MNPs with “stealth” components, they would survive endogenous clearance mechanisms (e.g., hepatic, splenic, renal) for a sufficiently long period of time to allow significant extravasation from the tumor vasculature. Nevertheless, using an identical protocol as for the previous experiment with the pyramid magnet, except that i.v. rather than i.p. administration was employed, we determined whether the current parameters of magnetic field strength and shape and MNPs might be effective. The results are shown in **Figure 4**. The images on the left are pre-injection, and those on the right are following 2 hr of magnetic vectoring; as before, the upper images are T2-weighted, and the lower, T2\*-weighted. Comparisons of the T2\*-weighted images, pre- vs. post-injection, are strongly indicative of tumor localization of the MNPs with this i.v. injection protocol.

**In summary**, from the last two experiments, we believe that more selective tumor localization of the MNPs is evident in the HEY model with the pyramid vs. the cylindrical magnet. Already, evidence is mounting that the design and selection of the magnetic vectoring device is an important parameter for optimizing MNP localization; ultimately, it also follows that the therapeutic efficacy vs. toxicity of drug-loaded MNPs will be similarly influenced. Further, although MR imaging has been an extremely valuable guide for protocol design, we emphasize that its resolution is not adequate to settle key questions of the actual location of the MNPs: peri-tumorally, within the tumor interstitial fluid but not internalized, or endocytosed by tumor/stromal cells. This information is key to development of a rationale for the design of the MNP pro-drugs to be used in the next phase of our studies; thus, the need for histological analysis of MNPs in tissue, of which fluorescence microscopy of MNP-FITC will be a component.

On the path to pre-clinical evaluation of MNP pro-drugs, our next steps will include optimizing the magnetic vectoring parameters of MNPs in the HEY peritoneal model, as well as in other human ovarian carcinoma i.p. xenograft models with a multi-focal presentation, more akin to carcinomatosis. Comparison of i.p. versus i.v. administration of MNPs is likely to give different outcomes in these models, due to the differences in the development of the tumor vasculature. We are mindful of the experience in the rabbit VX-2 tumor model, that indicated that only intra-tumor arterial administration of mitoxantrone-loaded MNPs was effective, whereas i.v. administration was totally ineffective (15-19). Since restriction to intra-tumor arterial administration has marked limitations in terms of clinical applicability, addressing the basis for such pre-clinical results should be a rewarding challenge. The principles of MNP vectoring as a basis for drug delivery are potentially applicable to other unmet clinical needs; this includes targeting adjuvant and neoadjuvant chemotherapy in localized breast cancer, so we will also evaluate MNP vectoring in orthotopic human breast adenocarcinoma models. In time, we will extend our studies to MNPs carrying a drug payload, and possibly an additional, affinity-based targeting moiety. These anti-tumor efficacy studies will include pharmacokinetic analyses of the MNPs as well as the released drugs, mindful of the unfortunate experiences that have occurred with other early efforts to bring magnetic vectoring of drugs to clinical utility (20-23).

### **Acknowledgements**

We would like to acknowledge grant support from the 2005 Department of Defense Breast Cancer Research Program and the Alliance for NanoHealth. The technical expertise of Mr. Edmond Auzenne, M.S. and Mr. Don Gibson, M.S., and the technical personnel in the MDACC Small Animal Imaging Facility are also acknowledged.

**References**

1. MM Fields, E Chevlen,,Clin J Oncol Nurs. 10 (2006) 77.
2. J Morrison, J Br Menopause Soc. 11 (2005) 66.
3. F Parazzini, F Chiaffarino, E Negri et al., Int J Gynecol Cancer. 14 (2004) 431.
4. P Kringen, Y Wang, V Dumeaux et al., BMC Cancer. 5 (2005) 134.
5. ER Greimel, V. Bjelic-Radisic, J Pfisterer et al., J Clin Oncol. 24 (2006) 579.
6. SK Chatterjee, BR Zetter. Future Oncol. 1 (2005) 37.
7. FM Kew, DJ Cruickshank. Int J Gynecol Cancer. 16 (2006) 380.
8. CS Chu, SC Rubin. Best Pract Res Clin Obstet Gynaecol. 20 (2006) 307.
9. RF Ozols. Semin Oncol. 33 (2006) 3.
10. C Bankhead. J Natl Cancer Inst. 98 (2006) 510.
11. E de Bree, H Rosing, J Michalakis et al. Eur J Surg Oncol. 2006 Apr 14 [Epub ahead of print]
12. DK Armstrong, B Bundy, L Wenzel et al., N Engl J Med. 354 (2006) 34.
13. G Lian, K Lewelling, M Johnson et al. Microsc Microanal 10 (2004).
14. W Yuill, CE Seeney, J Klostergaard. Abstract. 6<sup>th</sup> Intl Conf, "Scientific and Clinical Applications of Magnetic Carriers", Krems, Austria, May, 2006.
15. C Alexiou, W Arnold, RJ Klein et al., Cancer Res. 60 (2000) 6641.
16. AS Lubbe, C Alexiou, C Bergemann. J Surg Res. 95 (2001) 200.
17. C Alexiou, R Jurgons, RJ Schmid t al., J Drug Target. 11 (2003) 139.
18. C Alexiou, R Jurgons, R Schmid et al., HNO. 53 (2005) 618.
19. C Alexiou, RJ Schmid, R Jurgons t al., Eur Biophys J. 35 (2006) 446.
20. SR Rudge, TL Kurtz, CR Vessely et al., Biomaterials. 21 (2000) 1411.
21. SC Goodwin, CA Bittner, CL Peterson et al., Toxicol Sci. 60 (2001) 177.
22. S Rudge, C Peterson, C Vessely t al., J Control Release. 74 (2001) 335.
23. T Leakakos, C Ji, G Lawson t al., Cancer Chemother Pharmacol. 51 (2003) 445.

**Figure Captions**

**Figure 1: Coronal T1-weighted 3D images.** 150  $\mu$ L of 1000  $\mu$ g/ml concentrations of MNPs (silica-coated, single-domain, superparamagnetic magnetite nanoparticles, 15-20 nm diameter) were injected i.p. This was followed immediately by placement of a 22 mm diameter cylindrical Nd/B/Fe magnet (Arbor Scientific), rated at 5600 Gauss at its face surface, to the right of the mouse abdomen for 2 hr, with the mouse resting on its anterior under monitored isoflurane inhalation anesthesia. Control mice did not have a magnet in place, but otherwise were treated the same and for the same duration. 1) The MR image on the left is pre-injection; 2) the image in the middle is taken after a mouse was injected with MNPs and left under anesthesia with no magnet in place for 2 hr, showing wide dispersion of the MNPs remaining in the peritoneum; 3) the image on the right is from a mouse similarly injected, but with the magnet placed to the right

(left on image) of its abdomen. MRI evidence for accumulation of MNPs near the juxtaposed magnet is clear.

**Figure 2: Sagittal T1-weighted and T2\*-weighted images.** Mice were treated identically to the protocol described for Figure 1, except that i.p.-injected FITC-MNPs were employed, and the cylindrical Nd/B/Fe magnet was placed over the abdominal midline needle-track from i.p.-implantation of HEY tumor cells two weeks earlier. The two control images on the top are taken 2 hr post-injection, without a magnet in place over the anesthetized mouse: the T1-weighted image on the right showing the prominent outline of the tumor in the anterior abdominal wall, and the T2\*-weighted image on the left documenting absence of MNP accumulation in any tissue in this slice. The three images on the bottom are taken 2 hr post-injection with the magnet in place over the tumor of the anesthetized mouse for the full duration. The T2\*-weighted image on the left shows marked signal ablation due to MNP accumulation in the tumor/peri-tumoral area and neighboring abdominal wall. The yellow scalar is inserted for orientation of the distance between bladder and tumor centers on this image and the image in the middle. The two T1-weighted images in the middle and right display clear susceptibility artifacts characteristic of signal distortion due to USPIOs; the middle image again shows the yellow scalar for orientation, as well as a red marker for the tumor center, while the image on the right is native. MRI evidence that MNPs can be vectored to the HEY tumor/peri-tumoral area is clear.

**Figure 3: Sagittal T2-weighted and T2\*-weighted images.** This experiment followed a protocol identical to that for the experiment in Figure 2, with i.p. injection of MNPs, except that a pyramid-shaped magnet with a narrow  $\sim$ 3 mm square peak (K and J Magnetics) was employed. The images on the left vs. right are from neighboring slices; the upper images are T2-weighted; the lower images are T2\*-weighted. Compare these T2\*-weighted images to that on the bottom left of Figure 2; the use of the more focused magnet caused less undesired MNP localization to the normal tissues of the abdominal wall, while still achieving accumulation to the HEY tumor or peri-tumoral area.

**Figure 4: Sagittal T2-weighted and T2\*-weighted images.** This experiment followed a protocol identical to that for the experiment in Figure 3, except that MNPs were injected i.v. The images on the left are pre-injection; those on the right are taken after 2 hr of magnetic vectoring; upper images are T2-weighted, and the lower, T2\*-weighted. Comparisons of the T2\*-weighted images, pre- vs. post-injection, are strongly indicative of tumor localization of the MNPs with this i.v. injection protocol.

# Fig. 1

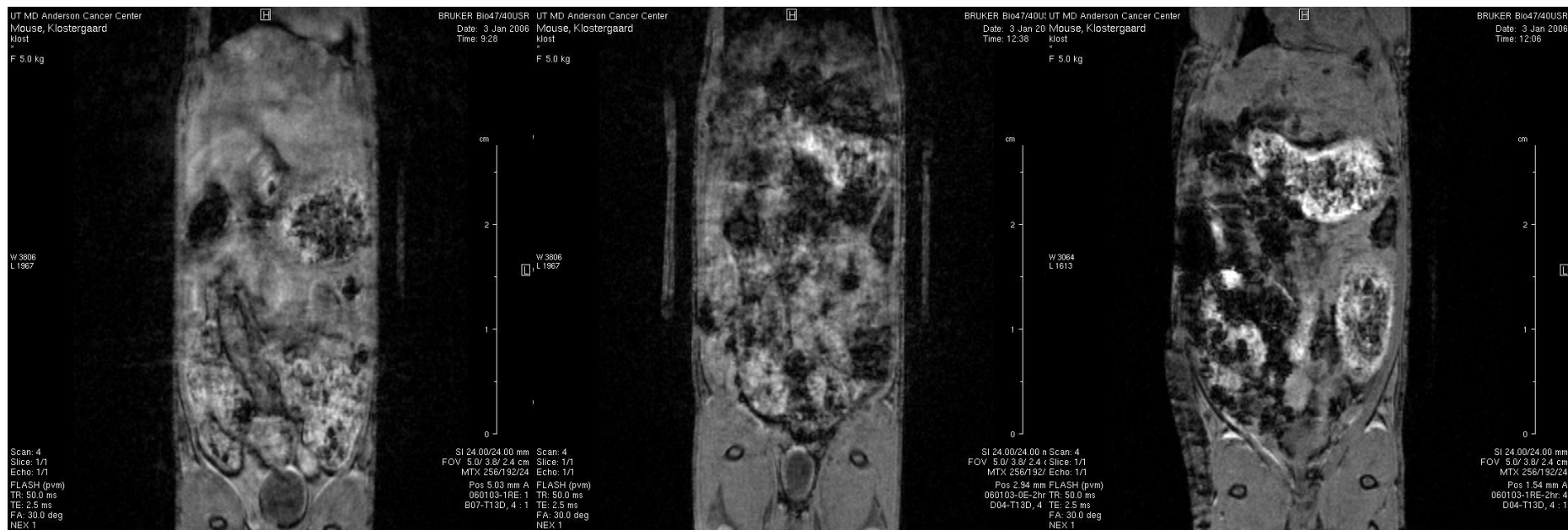


# Fig. 2

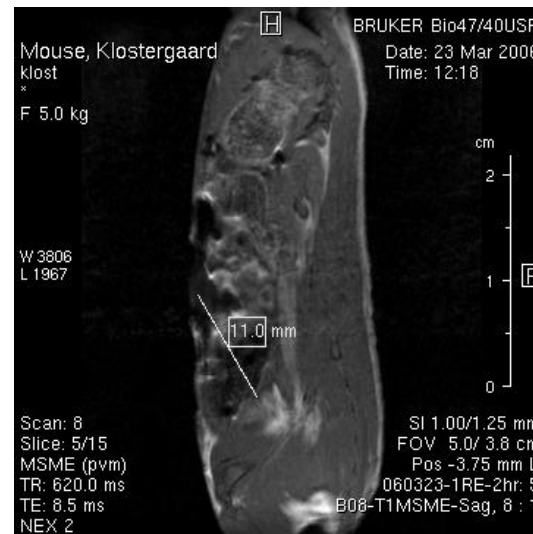
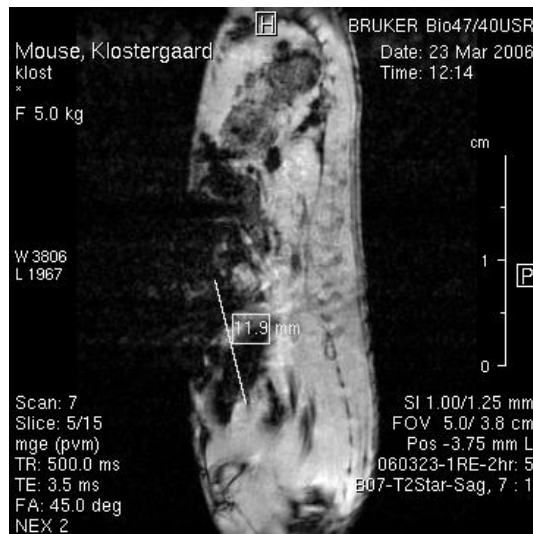
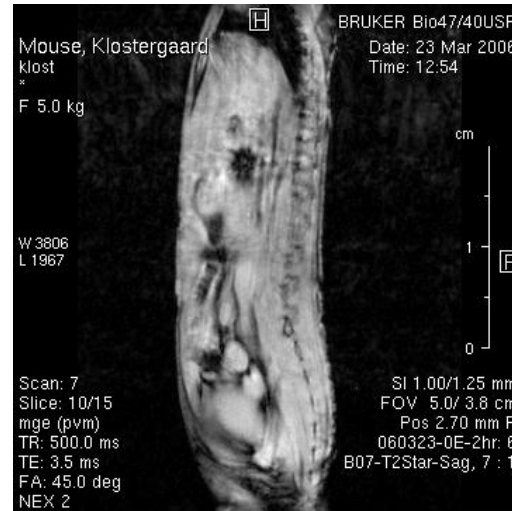


# Fig. 3

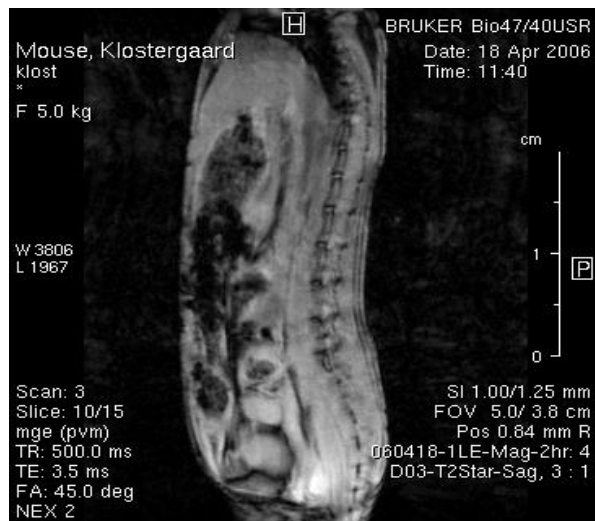
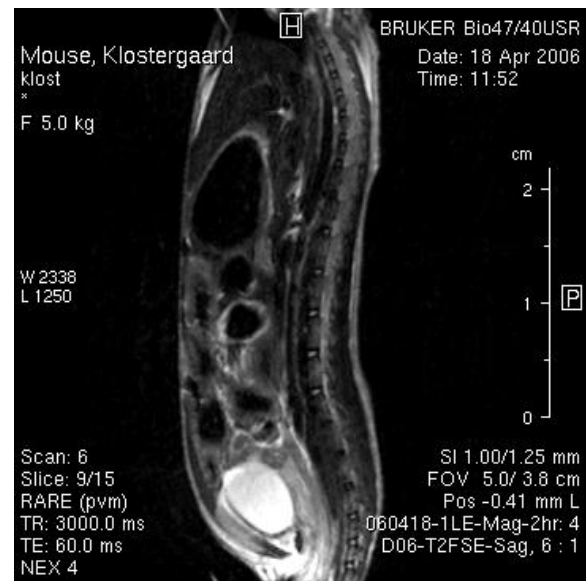
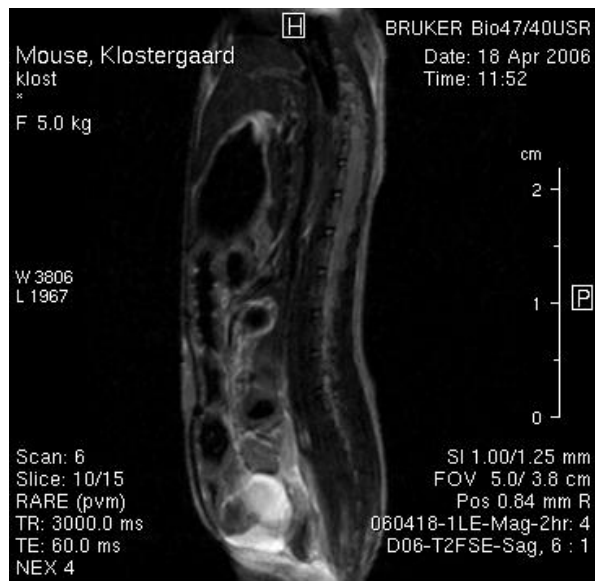


# Fig. 4

